Estimation of Surface Radiation and Energy Flux Densities from Single-Level Weather Data

WIM C. DE ROOY AND A. A. M. HOLTSLAG*

Royal Netherlands Meteorological Institute (KNMI), De Bilt, the Netherlands

(Manuscript received 27 December 1997, in final form 26 May 1998)

ABSTRACT

A scheme is proposed that relates surface flux densities of sensible heat, latent heat, and momentum to routine weather data. The scheme contains parameterizations concerning the radiation components and the surface energy flux densities. The parameterizations are developed and examined using observations from 1987 of a grass-covered surface at Cabauw in the Netherlands. It is shown that improvements in the parameterizations are achieved by incorporating an albedo dependence on solar elevation, a longwave downward radiation with a correction for the amount of high clouds, and a soil heat flux with a soil temperature approximated by a 24-h-mean 2-m temperature. In addition, the Penman–Monteith concept for the latent heat flux is utilized with a simple one-parameter surface resistance, which depends on atmospheric moisture deficit in particular. Special attention is paid to the treatment of surface inhomogeneities. A distinction is made between stable conditions, when measurements in the lower 10 m appear to be in equilibrium with the local surface, and unstable conditions, when measurements seem to be influenced by deviating upstream surface conditions. A constant roughness length for heat above grassland of 1 mm is applied. Finally, the scheme as a whole is evaluated and compared with a previous approach by A. P. van Ulden and A. A. M. Holtslag. It appears that in particular the sensible heat flux is improved with the new scheme. This can be ascribed mostly to the replacement of the modified Priestley–Taylor by the Penman–Monteith formulation and by a better representation of the surface temperature.

1. Introduction

Estimates of surface flux densities (hereafter referred to as fluxes) are valuable for many meteorological applications, for example, for air pollution studies and estimation of evaporation from vegetation in agriculture. Surface fluxes also appear as important scaling quantities in turbulence variables (Holtslag and Nieuwstadt 1986). However, surface fluxes data are not routinely available quantities. Therefore, we have developed a diagnostic scheme that relates surface fluxes of heat, water vapor, and momentum to readily available data, namely, routine weather observations or model output at a single level. The starting point for the development of such a scheme was presented by Holtslag and van Ulden (1983) and van Ulden and Holtslag (1985, henceforth UH85). Parameterizations of the radiation components and the surface energy fluxes included in the UH85 scheme as well as alternative parameterizations are evaluated in this study, in which we try to minimize the number of parameters and input variables.

The scheme presented here is evaluated with the use of an extensive dataset, covering many sorts of weather conditions. We use observations obtained in 1987 from and near the meteorological mast in Cabauw in the center of the Netherlands because this set has been well documented and evaluated by Beljaars and Bosveld (1997). Special attention is paid to the problem of how to deal with nonideal fetch conditions or surface inhomogeneities, such as observed around many synoptic stations. The Cabauw mast is situated in a typical moderately complex terrain; the measurements are made above a smooth grass-covered surface, but occasional upstream obstructions and rougher areas are present (van Ulden and Wieringa 1996). These upstream obstacles can cause deviations from the ordinary flux–profile relationships and an increase of shear stress with height.

Section 2 describes the basic concepts utilized in the current study, and section 3 summarizes the observations. Parameterizations concerning the radiation components are evaluated in sections 4 and 5, and formulations of the soil heat flux are examined in section 6. In the UH85 scheme, a modified Priestley–Taylor concept is used for the parameterization of the latent heat flux (λE). The performance of this concept is compared

* Additional affiliation: Institute for Marine and Atmospheric Research, University of Utrecht, Utrecht, the Netherlands.

Corresponding author address: Wim de Rooy, Royal Netherlands Meteorological Institute, P.O. Box 201, 3730 AE De Bilt, the Netherlands.
E-mail: rooyde@knmi.nl

TABLE 1. Summary of the paramaterizations investigated in this paper.

Section	Parameterized quantity	Method/alternatives
4	Surface temperature (T_0)	Monin–Obukhov similarity theory with various values for the roughness lengths of momentum and heat
4	Outgoing longwave radiation ($L^{\uparrow}$)	Stefan–Boltzmann law with different values for the emissivity of the surface
5a	Incoming longwave radiation ($L^{\downarrow}$)	Stefan–Boltzmann law with various formulations for the apparent emissivity of the atmosphere and corrections for clouds
5b	Albedo (r)	Constant or a function of the solar elevation and other factors
6	Soil heat flux (G)	Different forms of a linearized diffusion equation
7	Latent heat flux (λE)	Modified Priestley–Taylor or Penman–Monteith concept

with a Penman–Monteith approach in section 7. With the latter approach, two resistances need to be described, namely, the aerodynamic (r_a) and the surface resistance (r_s). Emphasis is put on an accurate description of these resistances, and different formulations of r_s are investigated. Finally, in section 8 the performances of the UH85 and the new scheme are compared. Table 1 provides an overview of the approaches in this study.

The proposed scheme requires at least the following input data: total cloud cover, wind speed at one level, time of the day, air temperature, and humidity. In addition the inputs of incoming solar radiation, fraction of low and middle cloud, as well as the mean temperature of the past 24 h is recommended. Further, surface characteristics such as albedo, roughness length, and thermal conductivity of the soil are used.

2. Concepts

a. Surface radiation and energy budget

The most important processes concerning estimation of surface fluxes from single-level weather data are presented schematically in Figs. 1a–c. In these figures, a distinction can be made between radiation and energy fluxes. The net radiation Q^* reads

$$Q^* = K^* + L^{\downarrow} - L^{\uparrow}, \tag{1}$$

with

$$K^* = K^{\downarrow}(1 - r), \tag{2}$$

where K^* is the net shortwave radiation, $L^{\downarrow}$ is the incoming longwave radiation, $L^{\uparrow}$ is the outgoing longwave radiation, $K^{\downarrow}$ is the downward shortwave radiation that

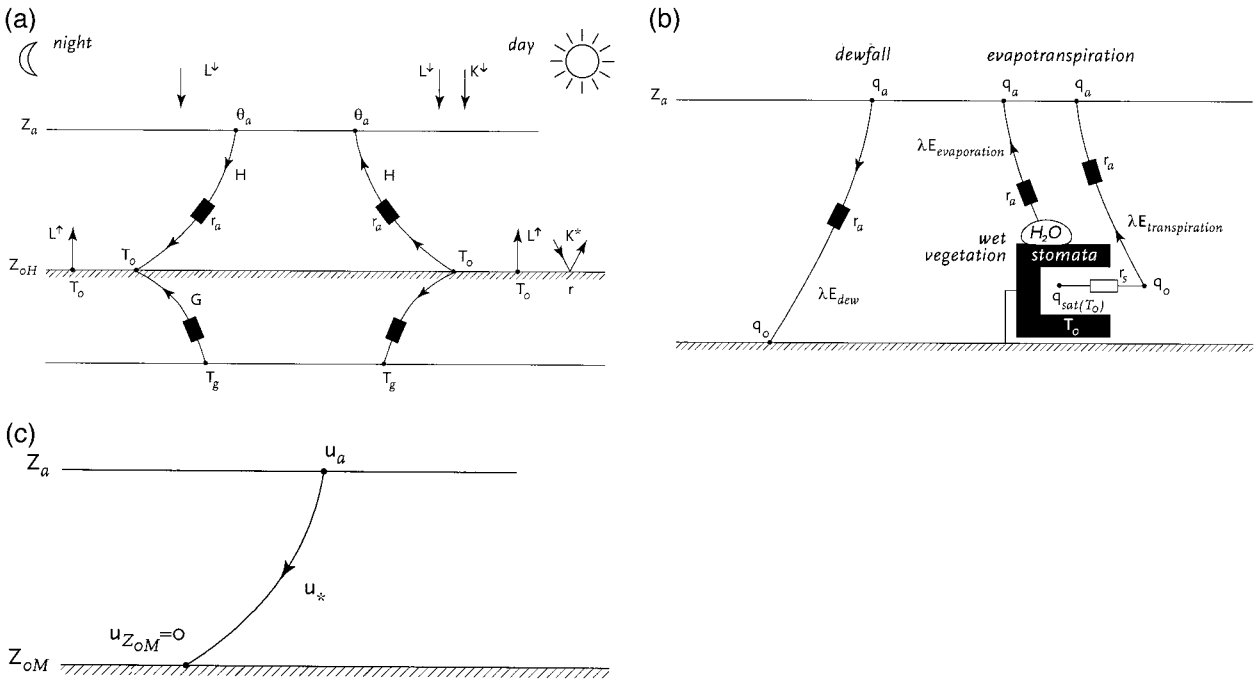

FIG. 1. (a) Radiation, sensible heat flux (H), and soil heat flux (G). Here $L^{\downarrow}$ and $L^{\uparrow}$ are the incoming and outgoing longwave radiation, $K^{\downarrow}$ is the incoming shortwave radiation, and K^* is the net shortwave radiation. Further, r is the albedo, T_0 is the surface temperature, and θ_a is the potential temperature at height z_a. Here T_g is a temperature in the soil, z_{0H} is the roughness length for heat, and r_a is the aerodynamic resistance. (b) Latent heat flux (λE). Here q_0 and q_a are the specific humidity at the surface and z_a, respectively; r_s is the surface resistance; and $q_{\text{sat}}(T_0)$ is the saturated specific humidity at temperature T_0. (c) Friction velocity (u_*). Here z_{0M} is the roughness length for momentum and u_a is the wind speed at height z_a.

originates from the sun, and r is the albedo of the surface. Normally, $K^{\downarrow}$ will be available by means of observations or model outputs. In that case, the accuracy of (2) will depend only on the parameterization of the albedo, which is the subject of section 5b. If, however, $K^{\downarrow}$ is not available, a parameterization can be applied (e.g., Holtslag and van Ulden 1983). In addition $L^{\downarrow}$ may be available from model outputs. Parameterizations of $L^{\uparrow}$ and $L^{\downarrow}$ are investigated in sections 4 and 5a, respectively.

The surface energy balance relates the net radiation to the energy fluxes. Assuming that no energy is stored or released within the canopy, the surface energy balance equation can be written as

$$Q^* = H + \lambda E + G, \tag{3}$$

where H is the sensible heat flux, λE is the latent heat flux, and G is the soil heat flux.

b. Surface radiation temperature

All energy fluxes on the right-hand side of (3) plus the outgoing longwave radiation are strongly influenced by the temperature T_0 at the effective radiation level (hereafter surface temperature). Hence, its estimation is one of the major issues of this paper. By applying the Monin–Obukhov similarity theory, the surface temperature can be extrapolated from a reference level z_a down to z_{0H} using

$$\theta_0 = \theta_a - \frac{\theta_*}{k}\left[\ln\left(\frac{z_a}{z_{0H}}\right) - \Psi_H\left(\frac{z_a}{L}\right) + \Psi_H\left(\frac{z_{0H}}{L}\right)\right], \tag{4}$$

with

$$L = \frac{u_*^2 T_a}{k\theta_* g} \tag{5}$$

and

$$u_* = ku_a\left[\ln\left(\frac{z_a}{z_{0M}}\right) - \Psi_M\left(\frac{z_a}{L}\right) + \Psi_M\left(\frac{z_{0M}}{L}\right)\right]^{-1}. \tag{6}$$

Here, θ_a is the potential temperature (°C) at observation height z_a (m) and θ_0 is the potential temperature of the surface radiation level. Both potential temperatures are here defined with respect to the local surface pressure, thus $\theta_0 = T_0$. Further, θ_* is a temperature scale (°C) defined by $\theta_* = -H(\rho c_p u_*)^{-1}$, where ρ is the air density (kg m^{-3}) and c_p is the specific heat (J kg^{-1} K^{-1}), k is the von Kármán constant, z_{0H} is the roughness length for heat (m), L is the Obukhov length (m), Ψ_H is the stability correction for heat (following Beljaars and Holtslag 1991), u_* is the friction velocity (m s^{-1}), g is the acceleration of gravity (m s^{-2}), u_a is the wind speed (m s^{-1}) observed at height z_a, z_{0M} is the roughness length for momentum (m), and Ψ_M is the stability correction for momentum (also taken from the form in Beljaars and Holtslag 1991). The roughness length z_{0M} defines the virtual height above the surface where the downward-extrapolated profile [using (6)] yields the surface value (zero for wind). Similarly, z_{0H} is taken such that downward extrapolation of (4) provides the effective temperature at radiation level.

When using the flux–profile relationships (4) and (6) for the estimation of the surface temperature in heterogeneous terrain, it is necessary to distinguish between profiles adjusted to the local surface and perturbed profiles. Terrain inhomogeneities—for example, relatively smooth areas relieved by rougher areas or occasional obstructions—are the cause of perturbed profiles. In the present study, measurements are used of the Cabauw observation site, which is situated in a moderately complex terrain and therefore representative of many sites where meteorological observations are gathered according to WMO requirements (e.g., Wieringa 1986).

Whenever the observations of wind speed and temperature at height z_a are in equilibrium with the surface, u_* and T_0 can be described with (6) and (4) in combination with local roughness lengths for momentum, $z_{0M\text{loc}}$, and heat, $z_{0H\text{loc}}$. These local roughness lengths depend only on the local surface cover, which for short grass corresponds to $z_{0M\text{loc}} \cong 0.01$ m. Furthermore, a ratio $z_{0M\text{loc}}/z_{0H\text{loc}} = 10$ is widely accepted for equilibrium conditions (Garratt and Hicks 1973) and will be used here. We refer below to the latter as the ''local'' method.

On the other hand, temperature and wind speed measurements influenced by inhomogeneities in the upstream surface cover can be related to the friction velocity and surface temperature by applying a mesoscale, or effective, roughness length for momentum, $z_{0M\text{eff}}$ (Wieringa 1986), and similarly an effective roughness length for heat, $z_{0H\text{eff}}$ (Beljaars and Holtslag 1991). Unfortunately, there is a high degree of uncertainty in particular for $z_{0H\text{eff}}$. We refer below to this as the ''meso'' method.

In section 4, we investigate the applicability of the local and meso approach and the correct value for z_{0H} in order to obtain an accurate estimate of T_0 with observations at standard synoptic height under different stability conditions. Subsequently, the surface temperature thus established is applied to the parameterization of $L^{\uparrow}$ in section 4, G in section 6, and r_a in section 7.

c. Resistances

The aerodynamic resistance r_a (Fig. 1b) represents the resistance for transfer of sensible heat and water vapor between the surface (of leaf and ground) and height z_a and is specified using Monin–Obukhov similarity theory by letting

$$r_a \equiv -\rho c_p \frac{\theta_a - \theta_0}{H} = \frac{1}{ku_*}\left[\ln\left(\frac{z_a}{z_{0H}}\right) - \Psi_H\left(\frac{z_a}{L}\right) + \Psi_H\left(\frac{z_{0H}}{L}\right)\right]. \tag{7}$$

The partitioning of the available energy, $Q^* - G$, over H and λE is investigated in section 7.

Apart from the aerodynamic resistance, the surface resistance r_s plays an important role in the parameterization of λE. The surface resistance is introduced in order to deal with the unknown specific humidity deficit at the surface, $\Delta q_0 = [q_{sat}(T_0) - q_0]$ (g kg^{-1}). Thus (e.g., Monteith 1981)

$$r_s \equiv \frac{\rho\lambda\Delta q_0}{\lambda E}, \tag{8}$$

where r_s represents the resistance for transfer of water from the saturated air inside stomata at temperature T_0 up to the surface of the leaves, and λ is the latent heat of water vaporization. The results of different parameterizations of r_s within the Penman–Monteith approach are compared with the modified Priestley–Taylor (MPT) concept (Priestley and Taylor 1972; De Bruin and Holtslag 1982).

3. Observations

The current observations were gathered at the 200-m tower and the micrometeorological field at Cabauw, the Netherlands. A general description of the observation site and the half-hourly data is given by van Ulden and Wieringa (1996). The surroundings of the mast consist of grassland, small villages, trees, and river dikes (see van Ulden and Wieringa 1996). The observations refer to the year 1987. The 1987 data from Cabauw is also used by Beljaars and Viterbo (1994) and in the Project for Intercomparison of Land-surface Parameterization Schemes (PILPS; Chen et al. 1997). Here we use the dataset revised and quality controlled by Beljaars and Bosveld (1997, hereafter BB97). Note that BB97 used a model to fill in the missing observations, whereas we select only optimum quality (no synthetic) data.

Parameters measured and used in this paper are temperature at levels ranging from 0.6 up to 80 m, specific humidity from 0.6 up to 10 m, and wind speed at 10 m. Furthermore, direct measurements of solar radiation ($K^{\downarrow}$), net radiation (Q^*), and upward ($L^{\uparrow}$) and downward ($L^{\downarrow}$) longwave radiation are available. BB97 checked these radiation measurements on internal consistency and they applied bias corrections if necessary. Unfortunately, cloud cover is not observed at Cabauw. Therefore total cloud cover and the fraction of middle- and low-level clouds in Cabauw are estimated by averaging the hourly observations reported at three surrounding synops stations. For example, the mean half-hourly data in Cabauw valid at 1015 UTC is approximated by the averaged cloud cover reported at 1000 UTC at the surrounding stations.

Surface fluxes of heat (H), latent heat (λE), and momentum (u_*^2) have been derived indirectly from observations with the profile method (e.g., Holtslag and van Ulden 1983), in which temperature and humidity measurements at 0.6 and 10 m, wind speed at 10 m, and an effective roughness length, z_{0Meff}, are combined with surface similarity functions [like (4) and (6) in section 2b]. The effective roughness length depends on season (two seasons, winter and summer, are distinguished) and wind direction, and is specified from a site-specific table (Beljaars 1987). With the help of the heat flux as derived from the profile method, H_{prof}, the latent heat flux can be computed from the surface energy balance: $\lambda E_{bal} = Q^* - G - H_{prof}$, where G is the observed soil heat flux. This is called the balance method for latent heat.

A second method we have used to obtain H and λE is the Bowen method (Oke 1978), which assumes that the diffusivities for heat and moisture are the same. The Bowen method uses wet- and dry-bulb temperature differences between 0.6 and 2 m. As a result, the Bowen fluxes are more local (see section 2b) than the profile fluxes. Furthermore, the Bowen method is less robust when the temperature or humidity difference becomes small (e.g., at sunrise or sunset) or during nighttime when instrument errors in Q^* and G are relatively large. Hence we prefer H and λE obtained with the profile and balance method, respectively. Latent heat fluxes obtained with the profile method are generally regarded as less accurate because of the uncertainties in the humidity measurements. However, during nighttime the profile method might be more reliable than the other methods mentioned above, again because of the relatively large instrument errors in $Q^* - G$ (Holtslag and De Bruin 1988).

Differences between H_{prof} and H_{Bow} of up to 200 W m^{-2} can be observed in cases with wind directions between 300° and 340°. This can be explained by the presence of an observation cabin that perturbs the flux–profile relationship and therefore H_{prof}. Hours with these erroneous H_{prof} observations are excluded from our study by allowing a maximum difference of 50 W m^{-2} between H_{prof} and H_{Bow}. In this way, exclusions occur only for wind directions between 300° and 340°. Overall, the two methods do agree with each other and with direct observations of the surface fluxes (Nieuwstadt 1978; Holtslag and van Ulden 1983).

Finally, the soil heat flux has been determined with the so-called Λ method (BB97; De Bruin and Holtslag 1982) and the Fourier method (BB97). The former method is a combination of the measured heat fluxes at 5- and 10-cm depth and the temperature difference and soil thermal conductivity between 0- and 2-cm depth. Possible effects of nonrepresentative soil properties near the temperature sensors are automatically taken care of (BB97). The Fourier method extrapolates the measured heat fluxes at 5- and 10-cm depth to the surface, applying Fourier transformations to measured time series.

4. The surface temperature and outgoing longwave radiation

The surface temperature T_0 plays an important role in most processes examined in this paper (section 2b).

TABLE 2. Errors (W m^{-2}) [bias and standard deviation (SD)] in the estimated outgoing longwave radiation, $L^{\uparrow}$, by applying eq. (9) and several estimates of T_0.

Method	Unstable $H_{prof} > 0$		Stable $H_{prof} < 0$	
	Bias	SD	Bias	SD
Meso $z_{0H} = z_{0Meff}/10$	1.3	5.4	8.9	5.0
Meso $z_{0H} = z_{0Meff}/100$	4.4	4.9	7.3	4.6
Meso $z_{0H} = z_{0Meff}/6400$	10.0	8.1	4.3	4.4
Meso $z_{0H} = 0.001$ m	3.7	**4.6**	7.7	4.5
Local $z_{0H} = 0.001$ m	7.6	6.9	6.2	**3.6**
Optimal	−0.2	4.9	3.6	3.3

Here T_0 is related to observations of the outgoing longwave radiation $L^{\uparrow}$ by utilizing

$$L^{\uparrow} = \varepsilon_s \sigma T_0^4 + (1 - \varepsilon_s) L^{\downarrow}, \quad (9)$$

where T_0 is the temperature at radiation level (K), ε_s is the emissivity of the surface, and $\sigma = 5.67 \times 10^{-8}$ (W m^{-2} K^{-1}) is the Stefan–Boltzmann constant. The last term in (9) represents the reflected downward longwave radiation. As mentioned in section 2b, we interpret the temperature at the effective radiation level as the surface temperature.

The T_0 inferred from (9) can be compared to estimates from using (4) in a downward extrapolation of T_{2m} to the surface. As such we utilize the local approach or the meso approach (section 2b).

In the local approach, we use observations of u_{10m} and θ and q at 2 and 0.6 m, and the local roughness lengths ($z_{0Mloc} = 10^{-2}$ m and $z_{0Hloc} = 10^{-3}$ m for short grass) to determine L_{loc} and θ_{*loc}. Subsequently z_{0Hloc}, L_{loc}, and θ_{*loc} are substituted in (4) to estimate T_0. Otherwise, it appears that the results for the local approach are not significantly changed if θ and q are taken at 10 and 0.6 m instead.

In the meso approach, surface-layer similarity theory is used to calculate L_{meso} and θ_{meso} with observations of the wind speed at 10 m (u_{10m}) and observations of θ and q at 10 and 0.6 m. Furthermore, an effective roughness length for momentum, z_{0Meff}, dependent on wind direction and season (Beljaars 1987) is applied, while the roughness length for heat, z_{0Heff}, is taken as a fraction of this z_{0Meff}. As mentioned before, the correct value of this fraction is uncertain. Therefore, different fractions mentioned in the literature are investigated, such as $z_{0Meff}/z_{0Heff} = 10$, 100, and 6400 (e.g., Garratt and Francey 1978; Beljaars and Holtslag 1991), and additionally also $z_{0Heff} = 10^{-3}$ m.

Surface temperatures resulting from the two different approaches are used to calculate the outgoing longwave radiation with (9) and $\varepsilon_s = 1$ (blackbody radiation). Next, these estimates of $L^{\uparrow}$ are compared with observations and the results are shown in Table 2. There is some uncertainty in the value of ε_s corresponding with grassland. Changing the value of ε_s affects the bias, but not the standard deviation (SD) of the error. Note that SD and bias are related to the root-mean-square (rms) error by $\text{rms}^2 = \text{SD}^2 + \text{bias}^2$.

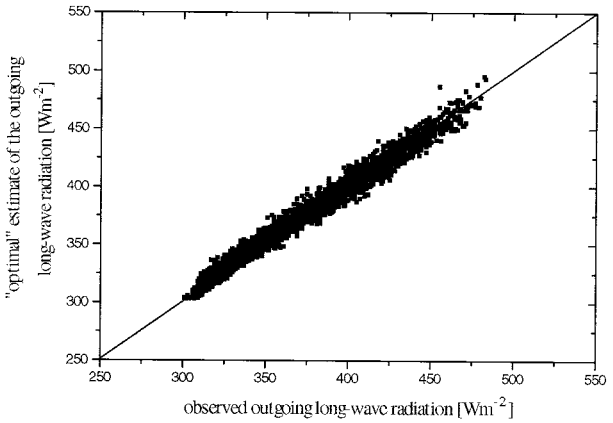

FIG. 2. Comparison of the observed outgoing longwave radiation with estimated values applying eq. (9) with the optimal method (7211 cases).

Results of experiments for unstable situations presented in Table 2 suggest that the meso approach in combination with $z_{0H} = 10^{-3}$ m gives the best results, that is, the smallest SD. This seems somewhat surprising because all observations are made below 10 m, where one might expect profiles adjusted to the local surface. However, in unstable conditions the strong mixing above the upstream rougher areas persists above the smoother observation area (Beljaars et al. 1983).

Results for stable situations shown in Table 2 clearly indicate that the local approach yields the best results. In contrast with unstable situations, temperature and wind profiles seem to be adapted to the local surface. At the observation point, measurements are made at a height below the internal boundary layer height for the smooth surface. If we assume that the heat flux is not affected by the varying roughness of the surface (Beljaars et al. 1983), it appears that during unstable conditions the eddy diffusivity adapts more slowly to the local surface behind a roughness transition than during stable conditions. This subject certainly requires further study.

On the basis of the current results (Table 2), the local approach will be applied during stable situations and the meso approach (with $z_{0H} = 10^{-3}$ m) during unstable conditions. To eliminate part of the bias in $L^{\uparrow}_{est}$, ε_s is optimized leading to $\varepsilon_s = 0.94$. For estimates of $L^{\uparrow}$ with $\varepsilon_s < 1$, observations of $L^{\downarrow}$ are used in (9). In comparison with values mentioned in the literature for ε_s for grassy vegetation (e.g., Oke 1978, $\varepsilon_s = 0.90$–0.95, for long to short grass, respectively) the emissivity found here is in agreement.

Results with $\varepsilon_s = 0.94$ in combination with a local approach during stable and a meso approach during unstable conditions are labeled as ''optimal'' in Table 2 and presented as a scatterplot in Fig. 2. With the optimal method, the quality of the $L^{\uparrow}$ estimates, and thus the

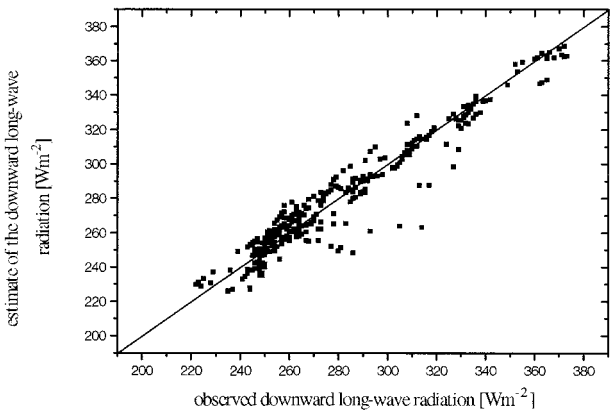

FIG. 3. Comparison of the observed downward longwave radiation with estimates applying eq. (10) with $\varepsilon_r = 1.2(e/T_{2m})^{1/7}$, $c_2 = 70$, and $c_3 = 50$ during clear-sky conditions ($N < 0.125$). The standard deviation (SD) = 9.0 W m^{-2} and the bias = -0.6 W m^{-2}.

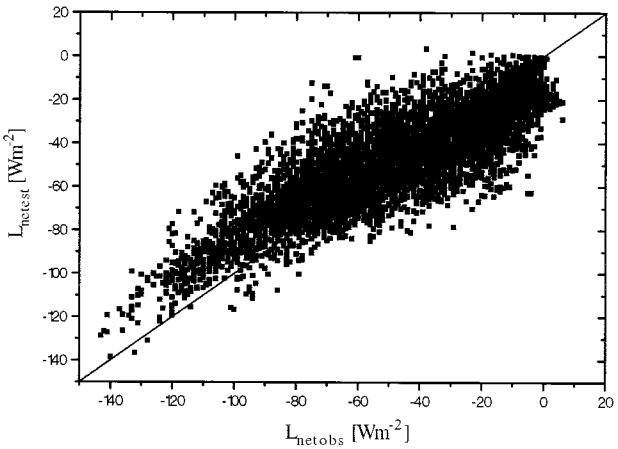

FIG. 4. Comparison of the observed net longwave radiation, L_{netobs} with estimates, L_{netest} applying eq. (10) with $\varepsilon_r = 1.2(e/T_{2m})^{1/7}$, $c_2 = 70$, and $c_3 = 50$. The SD = 16.0 W m^{-2} and the bias = -0.7 W m^{-2} (with $c_3 = 0$, i.e., no correction for high clouds, we obtain SD = 17.9 W m^{-2} and the bias = $+7.4$ W m^{-2}).

temperature at radiation level, are remarkably good (typical error in T_0 of less than 1°C). Note that the estimates and the measurements of $L^{\uparrow}$ are totally independent, and that the experiments cover a complete year, including very stable and unstable conditions with large temperature gradients between 2 m and the surface. Thus it appears that for all conditions in this dataset $z_{0H} \approx 10^{-3}$ m, whereas the appropriate value of z_{0M} varies with wind direction, season, and stability. As such the use of a specified value for z_{0M}/z_{0H} is not addressed by this analysis.

These results are important, not only for determination of T_0 for the evaluation of different parameterizations and the calibration of ε_s in (9), but they also indicate which approach (local or meso) is preferable for calculating the aerodynamic resistance in the Penman–Monteith (PM) formula.

5. Surface radiation budget

a. Longwave radiation

The incoming longwave radiation $L^{\downarrow}$ depends generally on the atmospheric profiles of temperature, humidity, liquid water, and other factors. This information is available in atmospheric models, and therefore $L^{\downarrow}$ may be taken from model outputs or directly from observations. However, typically $L^{\downarrow}$ is not available as a routine quantity. A simple parameterization of $L^{\downarrow}$ in terms of routinely available data is given by

$$L^{\downarrow} = \varepsilon_r \sigma T_r^4 + c_2 N - c_3(N - N_h), \qquad (10)$$

where ε_r is the apparent emissivity of the atmosphere; T_r is the air temperature at reference height, z_r; N is the total cloud cover; N_h is the fraction of low- and middle-level cloud; and c_2 and c_3 are empirical coefficients. The third term on the right-hand side in (10) accounts for the contribution of high clouds (Paltridge and Platt 1976). If the cloud cover N consists of only high clouds, N_h is zero and $L^{\downarrow}$ is lower than in the presence of low and middle clouds, as the temperature of high clouds is lower than the temperature of middle- and low-level clouds.

In the literature, different values for c_2 and c_3 are mentioned (see, e.g., Paltridge and Platt 1976). Also, several expressions for ε_r have been published. Some of these expressions include the effect of atmospheric humidity, while others are only dependent on temperature. Optimal values for c_2, c_3, and ε_r can be different from place to place. During experiments with different expressions for $L^{\downarrow}$ (Paltridge and Platt 1976; Brutsaert 1982; UH85) in combination with an optimal estimate of $L^{\uparrow}$ according to section 4, we noticed that all these parameterizations underestimate the values of net longwave radiation near zero, whereas they overestimate the more negative values. The former error is most evident if ε_r is a function of only temperature. The latter error is reduced if a correction for high clouds is included.

For the present dataset, relatively accurate results (Figs. 3 and 4) can be obtained with (10), where $c_2 = 70$ W m^{-2}, $c_3 = 50$ W m^{-2}, and $\varepsilon_r = 1.2(e/T_{2m})^{1/7}$ (after Brutsaert 1982), where e is the water vapor pressure (mbar) at 2 m. Figure 3 shows the result for $L^{\downarrow}$ during clear-sky conditions ($N < 0.125$). Figure 4 presents for all hours the result for $L_{net} = L^{\downarrow} - L^{\uparrow}$ (with optimal estimates of $L^{\uparrow}$ according to section 4).

The fact that the cloud cover in Cabauw is estimated by averaging the observed cloud cover at three surrounding stations probably deteriorates the results for $L^{\downarrow}$.

b. Solar radiation and albedo

We assume that solar radiation ($K^{\downarrow}$) is measured or available by other means (e.g., Holtslag and van Ulden

1983). Then the remaining quantity to be prescribed is the reflected radiation ($K^{\uparrow}$) or albedo ($K^{\uparrow}/K^{\downarrow}$). We examine two different parameterizations of the albedo. First, we adopt $r = 0.23$, which is a normal value for short grass (Oke 1978). Second, we investigate a formulation for the albedo dependent on the solar elevation φ, which has been suggested by Duynkerke (1992) and Beljaars and Bosveld (1997) for the Cabauw site:

$$r = 0.33 - 0.13 \sin\varphi - \left(\frac{K^{\downarrow}_{\text{dif}}}{K^{\downarrow}} - 0.1\right)\frac{(0.0867 - 0.13 \sin\varphi)}{0.9}. \quad (11)$$

Here $K^{\downarrow}_{\text{dif}}$ is the diffuse downward solar radiation, and the term 0.9 is included in (11) to make the formula independent of φ when $K^{\downarrow}_{\text{dif}} = K^{\downarrow}$. The fraction of diffuse radiation is estimated from the atmospheric transmissivity τ_a (Fig. 3.2 in Goudriaan and van Laar 1994):

$$\frac{K^{\downarrow}_{\text{dif}}}{K^{\downarrow}} = \begin{cases} 1, & \tau_a < 0.3, \\ 1.6 - 2\tau_a, & 0.3 < \tau_a < 0.7, \\ 0.2, & \tau_a > 0.7. \end{cases} \quad (12)$$

The atmospheric transmissivity, in turn, is approximated by

$$\tau_a = \frac{K^{\downarrow}}{1367 \sin\varphi}. \quad (13)$$

Observations of $K^{\downarrow}_{\text{dif}}$ show considerable scatter when compared with estimates using (12) and (13) with the observed $K^{\downarrow}$. However, if we use observations of $K^{\downarrow}_{\text{dif}}$ instead of estimates in our evaluation, the performance of (11) shows no significant change. So (12) and (13) can be accepted for the estimation of $K^{\downarrow}_{\text{dif}}$.

Because measurements of the net shortwave radiation K^* are not available in the 1987 dataset, the parameterization of the albedo has to be evaluated in terms of the net radiation Q^*. In other words, observations of $L^{\uparrow}$, $L^{\downarrow}$, and $K^{\downarrow}$ are used in combination with an approximation of the albedo in order to estimate the net radiation [(1) and (2)]. From Fig. 5, where the SD in Q^* is plotted, it becomes clear that applying (11) instead of a constant albedo can be expected to be superior in winter months when the solar elevation is low. Experiments using 1 yr of half-hourly observations reveal a bias of +3.6 and an SD of 12.6 W m^{-2} with the constant albedo, whereas the albedo applying (11), (12), and (13) results in a bias of +1.6 and an SD of +11.1 W m^{-2} in Q^*.

Because of the overall performance improvement, (11), (12), and (13) are selected for the parameterization of the albedo.

6. The soil heat flux

The soil heat flux is the downward heat flux that leaves the radiation level, passes through a layer of air and vegetation, and goes into the ground. Based on the fact that the layer of air and vegetation has a high resistance and low heat capacity, van Ulden and Holtslag (1985) proposed the following simple approximation for G:

$$G = -A_G(T_r - T_0), \quad (14)$$

where A_G is an empirical coefficient for soil heat transfer [e.g., 5 (W m^{-2} K^{-1}) for short grass (UH85)], T_r is a reference temperature, and T_0 is the temperature at radiation level. Here the idea is that T_r resembles a temperature not too deep in the soil.

To evaluate (14), we use T_0 determined as described in section 4 and different options for T_r. Van Ulden and Holtslag suggest taking T_r at a suitable reference level in the atmosphere. Here we experiment with the observed instant temperature at different heights (up to 80 m). Additionally we define T_r as the average $T_{2\text{m}}$ of the last 24 h, reflecting the time history of the atmosphere acting on the soil at the specific location. To realize a straightforward comparison, the results of all experiments concerning the parameterization of the soil heat flux are restricted to hours where all half-hourly measurements of $T_{2\text{m}}$ are available during the past 24 h (a total of 1479 cases for 1987).

With $T_r = T_{2\text{m}}$ and $A_G = 5$ W m^{-2} K^{-1}, negative (nighttime) values of G are overestimated and positive (daytime) values are underestimated (SD = 17.1 W m^{-2}). Apparently, $T_r = T_{2\text{m}}$ simulates a too-shallow soil temperature. Obviously, this problem can be reduced by increasing A_G. For $T_r = T_{2\text{m}}$ the optimal value reads $A_G = 9$, which reduces the error in G to SD = 15.42 W m^{-2}. Another approach is to simulate a deeper soil temperature by using an observed temperature at a higher altitude (with $T_r = T_{80\text{m}}$ and $A_G = 5$, we obtain SD = 15.9 W m^{-2}). However, the best results are achieved when $A_G = 5$ and T_r is taken as a 24-h mean of the observed 2-m temperature (SD = 12.0 W m^{-2}). The results for the latter parameterization are presented in Fig. 6.

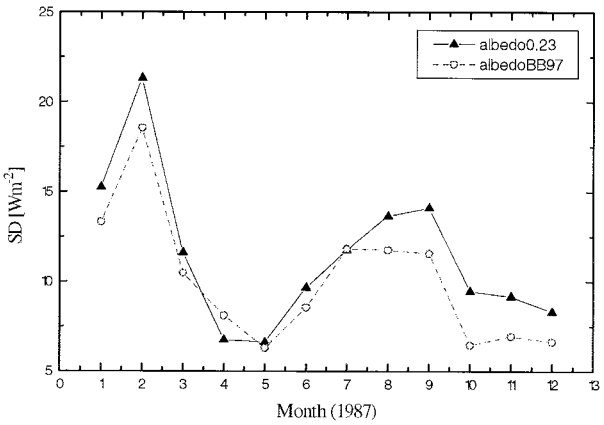

FIG. 5. The SD in the estimated Q^* using a constant albedo (albedo0.23) or (11) (albedoBB97) as a function of the month of the year.

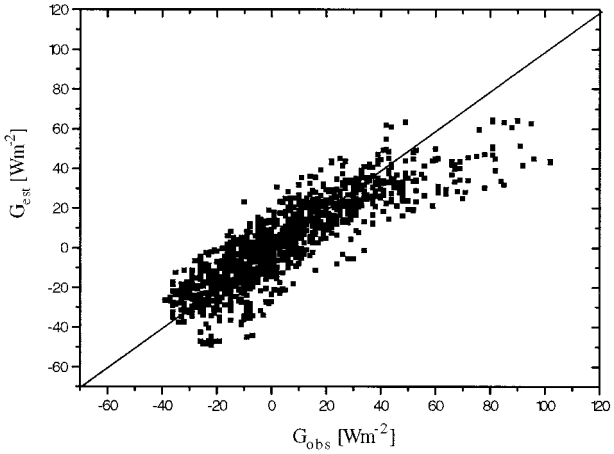

FIG. 6. Comparison of the observed soil heat flux (G_{obs}) with estimates (G_{est}) using (14), where T_r is the 24-h-mean temperature at 2 m, T_0 is determined according to section 4, and $A_G = 5$ W m^{-2} K^{-1}. The SD = 12.0 W m^{-2} and the bias = -1.4 W m^{-2}.

It appears that for all parameterizations, high values of the observed G are typically underestimated. It is difficult to determine the accuracy of these, indeed extremely high, observations. A possible explanation for the underestimation is that the sensor for the soil temperature at 0-cm depth [all high values of G are obtained with the Λ method (section 3)] is directly heated by solar radiation, for example, due to cracks in the ground during a dry period. In that case, the actual soil heat flux is overestimated by the observations.

7. Sensible and latent heat fluxes

a. Basic formulations

While the preceding sections consider the parameterization of the available energy $Q^* - G$, in this section we examine the partitioning of the available energy over H and λE. According to Slatyer and McIlroy (1961) and Monteith (1981)

$$\lambda E = \frac{s(Q^* - G)}{s + \gamma} + \frac{\rho c_p(\Delta q_a - \Delta q_0)}{(s + \gamma)r_a}, \qquad (15)$$

and

$$H = \frac{\gamma(Q^* - G)}{s + \gamma} - \frac{\rho c_p(\Delta q_a - \Delta q_0)}{(s + \gamma)r_a}, \qquad (16)$$

where s is the slope of the saturation specific humidity curve $\partial q_{sat}/\partial T$ at T_a; Δq_0 and Δq_a are the humidity deficit at the surface and measuring height, respectively; γ is the psychrometer constant; and r_a represents the aerodynamic resistance for transfer of sensible heat and water vapor between the surface (of leaf and ground) and the height of observation.

Considering (15) and (16) there are two unknowns that are studied here, namely, r_a and Δq_0. These are generally complicated factors, which may relate to many processes. Priestley and Taylor (1972) simplify (15) and (16) by relating the second term on the right-hand side to the first term on the right-hand side. In a modified Priestley–Taylor (MPT)concept, the second term on the right-hand side of (15) is taken as a positive constant, often called β ($\approx$20 W m^{-2}; De Bruin and Holtslag 1982). Further, an empirical parameter α, the so-called Priestley–Taylor parameter, is added:

$$\lambda E = \alpha\frac{s(Q^* - G)}{s + \gamma} + \beta. \qquad (17)$$

The MPT concept has been refined somewhat by van Ulden and Holtslag (1985, MPTUH85), who present β as a constant times the friction velocity u_*. In this way, u_* partly accounts for the effect of r_a on the aerodynamic evaporation [the last term on the right-hand side of (15) and (16)].

Here we also explore direct use of (15) and (16) by estimating r_a and Δq_0 (the PM concept). The aerodynamic resistance can be specified using Monin–Obukhov similarity theory (7). As mentioned before, a proper choice of z_{0H} is very important. Considering the results in section 4, we use $z_{0H} = 10^{-3}$ m for the surface covered with short grass in Cabauw. Apart from z_{0H}, r_a is determined by the formulation of the stability correction and the values of u_* and L. Again based on the results of section 4, we apply the local approach during stable and the meso approach during unstable conditions. In the overall scheme, r_a is determined in a similar way, again applying Monin–Obukhov similarity theory and making a distinction between stable and unstable conditions (but this time using observations at only one level).

b. The surface resistance

To estimate Δq_0 we may introduce the surface resistance r_s by (8). Typically for the Cabauw site, $r_s \approx 60$ s m^{-1} near noontime under well-watered soil conditions (De Bruin and Holtslag 1982). Generally r_s may depend on many factors. Here we investigate several formulations. As such we follow the so-called top–down approach, in which the surface resistance is diagnosed from measurements that are taken well above the vegetation without considering the details of the plant physiology (Baldocchi et al. 1991). We neglect bare soil evaporation, which is probably not important at the Cabauw location (BB97). In the following, the examined formulations for r_s are introduced and subsequently recited in Table 3a.

Jarvis (1976) recommends modeling r_s with

$$r_s = \frac{r_{s\min}}{\mathrm{LAI}} F_{\mathrm{SR}}^{-1} F_{\mathrm{MC}}^{-1} F_{\mathrm{VP}}^{-1} F_{\mathrm{AT}}^{-1}, \qquad (18)$$

and

$$F_{\mathrm{VP}} = \frac{1}{1 + a_q(\Delta q_a - \Delta q_r)}, \qquad (19)$$

TABLE 3a. Examined parameterizations for the latent heat flux.

Concept	Formulation
Modified Priestley–Taylor (17)	With $\alpha = 1$ and $\beta = 20$ W m^{-2} (MPT)
(No surface and aerodynamic resistance involved)	With $\alpha = 1$ and $\beta = 0.033u_*$ W m^{-2} (MPTUH85) $u_{*\text{loc}}$ during stable conditions and $u_{*\text{meso}}$ during unstable conditions (see section 4)
Penman–Monteith (PM) (15), (16), (7), and (8)	$r_s = 60$ s m^{-1}
r_a according to section 4 (local approach during stable and meso approach during unstable conditions)	r_s = Jarvis, i.e., (18) with functions optimized according to BB97 except for F_{MC} (here $F_{\text{MC}} = 1$)
	$r_s = 10\Delta q_{2\text{m}}$
	$r_s = 15 + 7\Delta q_{2\text{m}}$

where $r_{s\text{min}}$ is the minimum stomatal resistance; LAI is the leaf area index; and F_{SR}, F_{MC}, F_{VP}, and F_{AT} are empirical functions of, respectively, solar radiation, soil moisture content, vapor pressure deficit, and air temperature. Further, a_q and Δq_r are empirical constants. Formula (18) has been optimized for the 1987 dataset by BB97. Here we use their optimization for the F functions. Since the 1987 dataset contains mostly hours with sufficient soil water (BB97), we take at all times $F_{\text{MC}} = 1$. This greatly simplifies the use of (18) since soil moisture is not a routine variable, although we realize that this may need further analysis for dry soil conditions. Formally, we can rewrite (18) with the help of (19) as

$$r_s = a + b\Delta q_a. \tag{20}$$

Here a and b are parameters that relate to the original F functions of (18) and (19) by

$$a = \frac{r_{s\text{min}}}{\text{LAI}F_{\text{SR}}F_{\text{MC}}F_{\text{AT}}}(1 - a_q\Delta q_r) \quad \text{and}$$

$$b = \frac{r_{s\text{min}}a_q}{\text{LAI}F_{\text{SR}}F_{\text{MC}}F_{\text{AT}}}.$$

For the 1987 Cabauw data over grassland we find the somewhat surprising result that the combination of factors as given in a and b is rather constant. This indicates that r_s is mostly determined by Δq_a in our case. With typical values for $r_{s\text{min}}$, LAI, Δq_r, and the other factors in a and b (see BB97), we find that $a \cong 15$ s m^{-1} and $b \cong 7$ s kg m^{-1} g^{-1}. We also experiment with an even simpler form (requiring $a = 0$), namely,

$$r_s = \dot{b}\Delta q_a, \tag{21}$$

in which case we let $\dot{b} = 10$ s kg m^{-1} g^{-1}.

TABLE 3b. Errors (W m^{-2}) [bias and standard deviation (SD)] in the estimated λE or H for dry vegetation [hours between 0900 and 1600 UTC with no rain and $\Delta q_{2\text{m}} > 3$ (g kg^{-1})]. For an explanation of the examined parameterizations, see Table 3a. Note that (bias in H) = −(bias in λE) and (SD in H) = (SD in λE).

	Estimate against H_{prof} or λE_{bal}	
r_s or MPT	Bias (H)	SD
MPT with $\beta = 20$ and $\alpha = 1$	+6.6	29.3
MTPUH85 with β = constant(u_*) and $\alpha = 1$	+9.6	28.3
$r_s = 60$	+9.3	37.2
r_s = Jarvis	−7.4	30.2
$r_s = 10\Delta q_{2\text{m}}$	−1.1	26.8
$r_s = 15 + 7\Delta q_{2\text{m}}$	−0.6	28.0

c. Comparison and results

To investigate the performance of the various proposals, we divide the observations in two selections. First we consider hours between 0900 and 1600 UTC with no rain and $\Delta q_{2\text{m}} > 3$ (g kg^{-1}). This selection is thought to provide cases with dry vegetation. The additional advantage of selecting these hours of the day (without sunrise or sunset hours) is that the observations of λE obtained with the Bowen method can be used as a check, next to the balance method observations. The results for dry vegetation with the examined parameterizations for λE are presented in Table 3b. Measurements of $(Q^* - G)$ are used for λE_{est} as well as for the observations λE_{Bow} and λE_{bal}. In this way possible errors and biases in the observed $(Q^* - G)$ (section 6) have no effect on the results in Table 3b.

We note that using a constant value for r_s results in a significant SD. We also see that including the BB97 calibration of the Jarvis formula yields an SD very similar to the MPT approach. During experiments we noticed that the results for small λE are rather insensitive to the formulation of r_s. However, for larger values of λE, formulations dominated by the $\Delta q_{2\text{m}}$ dependence show less scatter.

How can we explain the good results of Table 3b with the simple estimate of surface resistance depending on humidity deficit only? Normally Δq_a increases during the day, which correlates well with the observed average diurnal change of the surface resistance (a minimum in the early day and an increase throughout the afternoon) observed above different vegetations (e.g., BB97; Monteith 1995). A possible explanation for the observed diurnal change of the surface resistance can be found in the drying of the soil immediately adjacent to the

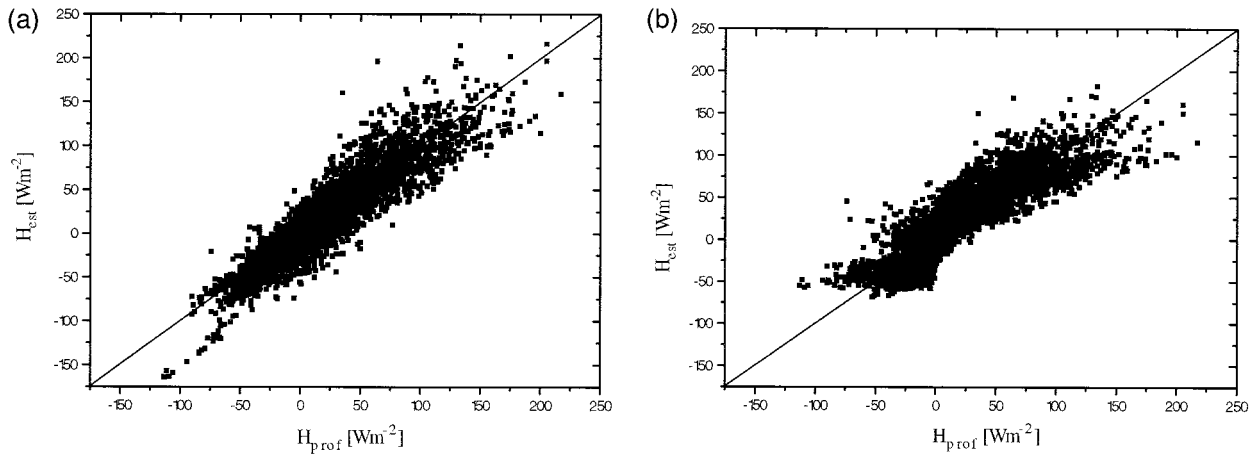

FIG. 7. (a) Comparison of the observed heat flux (H_{prof}) with estimates (H_{est}), applying (16) and (7) with $r_s = 10\Delta q_{2\text{m}}$ and the observed ($Q^* - G$) as input. The SD = 15.7 W m^{-2} and the bias = -2.8 W m^{-2}. (b) Comparison of the observed heat flux (H_{prof}) with estimates (H_{est}), applying the MPT approach and the observed ($Q^* - G$) as input. The SD = 20.0 W m^{-2} and the bias = -4.8 W m^{-2}.

roots during the day. At night the well-watered situation is restored, leading to a minimum resistance in the early morning (F. C. Bosveld 1997, personal communication).

Another argument for the good performance of an r_s formulation with a strong Δq_a dependence can be found in its behavior in situations with either wet vegetation or dry soil. If the soil is dry, Δq_a is normally large, resulting in a large r_s and thus a significant reduction of λE. On the other hand, in situations with wet vegetation [very common in Cabauw (BB97)] Δq_a and r_s will be small. In addition we may note that for grass typically $r_a > r_s$, which means that the flux estimates are not that sensitive to detailed specification for r_s.

We now address the performance of the parameterizations under all circumstances (7211 cases). This means that also hours with partly or complete wet vegetation are included in the evaluation. Again we compare estimates of H and λE with H_{prof} and λE_{bal} observations. The results reveal that the MPTUH85 approach, with the u_*-dependent β parameter, achieves better results than the MPT concept, in particular during nighttime (SD of 16.6 and 20.0 W m^{-2}, respectively). Furthermore, the Jarvis formulation leads to an SD of 18.4 W m^{-2}. Again, the parameterization $r_s = 10\Delta q_{2\text{m}}$ provides the smallest SD (15.7 W m^{-2}). Therefore this parameterization is selected for the new scheme.

In Figs. 7a and 7b scatterplots of H_{prof} against H_{est} with, respectively, $r_s = 10\Delta q_{2\text{m}}$ and the MPT approach are shown. We plot only the sensible heat flux because differences between the approaches are illustrated most clearly with scatterplots of H, as H is typically a smaller term than λE. An interesting result of the evaluation experiments is that different parameterizations of r_s give almost the same latent heat flux for small values of λE. However, the impact of different r_s parameterizations on large values of λE (>200 W m^{-2}) and on the complete range of H values can be quite significant, especially at high wind speeds (low r_a).

In contrast to the observations, the MPT concept produces only values of H in the range -60 W m$^{-2} < H < +170$ W m^{-2} (Fig. 7b). Why is H when used in the MPT concept so constrained?

Strong negative values of H are observed when the aerodynamic evaporation [last term on the right-hand side of (15)] is large, leading to a relatively large positive λE. In the MPT concept the aerodynamic evaporation is limited because it is assumed to be constant or only dependent on u_* (UH85). In practice, and in the PM concept, the aerodynamic evaporation is also influenced by the atmospheric demand for evaporation [proportional to $(\Delta q_a - \Delta q_0)$]. Incidentally, due to the radiation dependence, a Jarvis-type surface resistance becomes very large during nighttime; consequently, the lower limit in the estimated H is also present with the Jarvis formulation.

The results of Fig. 7a with $r_s = 10\Delta q_{2\text{m}}$ show an underestimation for strong negative values of H. All these strong underestimations occurred on 27 and 28 February 1987 during a near gale (observed $u_{10\text{m}} \approx 17$ m s^{-1}). For some hours during this near gale, the reported H_{Bow} is significantly lower (down to -150 W m^{-2}) than H_{prof}. Therefore, we do not expect that these underestimations of very low H are systematically associated with the use of $r_s = 10\Delta q_{2\text{m}}$.

In the MPT formulation, the upper limit in the estimated H is caused by the reduction of H at high temperatures due to the temperature dependence of the $[1 - s/(s + \gamma)]$ term. Because in practice high values of H_{prof} tend to correspond to high temperatures, the upper limit is recognizable in scatterplots of H_{est} against H_{prof} (see Figs. 7b and 8b cited below).

8. Comparison with a previous approach

Based on the results of the preceding sections, a synthesis is made of parameterizations, henceforth called

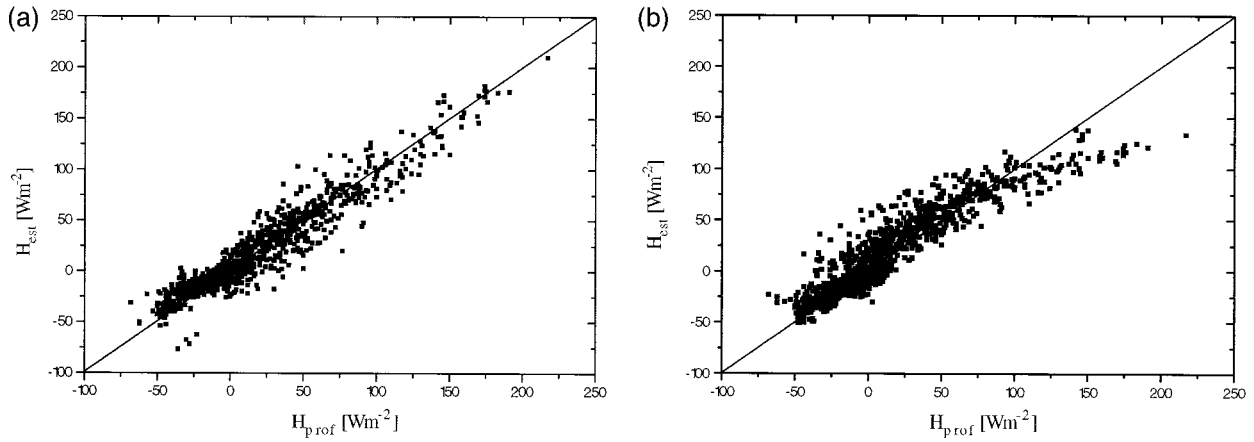

FIG. 8. (a) Comparison of the observed heat flux (H_{prof}) with estimates (H_{est}) using the new scheme. The SD = 11.8 W m^{-2} and the bias = +1.6 W m^{-2}. The SD of H_{prof} vs H_{Bow} = 11.7 W m^{-2}. (b) Comparison of the observed heat flux (H_{prof}) with estimates (H_{est}) using the UH85 scheme. The SD = 15.6 W m^{-2} and the bias = +2.5 W m^{-2}.

the new scheme, which provides surface fluxes with standard synoptic data as input. A technical description of the model setup is presented in the appendix. In the evaluation presented here, the new scheme uses the following input: q_{2m} (g kg^{-1}), T_{2m} (°C), N (fraction), N_h (fraction), 24-h-mean 2-m temperature (°C), u_{10m} (m s^{-1}), and $K^{\downarrow}$ (W m^{-2}). The performance of the new scheme is compared with the UH85 scheme, also published as a software package (Beljaars et al. 1989; Beljaars and Holtslag 1990). The latter scheme uses: T_{2m} (°C), N (fraction), u_{10m} (m s^{-1}), and $K^{\downarrow}$ (W m^{-2}). In Table 4, the site-specific surface parameters for the new and the UH85 scheme are recited.

As in section 6, only concatenated 24-h temperature measurements are used for the determination of the 24-h-mean 2-m temperature. Mainly because of this restriction, only 1453 cases are included in the evaluation. However, these 1453 cases still represent a broad range of weather conditions. We distinguish three classes in our evaluation according to solar elevation φ and surface heat flux derived from the profile method H_{prof}:

- nighttime, stable, hours $\varphi < 0$ and $H_{prof} < 0$ (595 cases),
- transition hours $\varphi \geq 0$ and $H_{prof} \leq 0$ (267 cases),
- daytime, unstable, hours, $\varphi > 0$ and $H_{prof} > 0$ (590 cases).

Figures 8 and 9 show the sensible and latent heat fluxes as determined from the observations and the new and UH85 schemes, which cover all three classes.

The results of both schemes for H during nighttime are comparable. However, this evaluation contains no $H_{prof} < -70$ (W m^{-2}), this is probably in favor of the UH85 scheme because in Cabauw this scheme is not capable of producing $H_{est} < -70$ W m^{-2} (section 7). For nighttime, stable hours, latent heat fluxes obtained with the profile method are considered to be more reliable than fluxes derived from the Bowen ratio method (Holtslag and De Bruin 1988). Compared against λE_{prof}, the new scheme shows a much better performance than the UH85 scheme (SD of 6.1 instead of 9.3 W m^{-2}).

As suggested in section 4, the new scheme uses a local approach during stable conditions. Experiments under stable conditions with the new scheme in combination with a meso approach ($z_{0M} = z_{0Meff}$ and $z_{0Heff} = 10^{-3}$ m) leads to worse estimates (especially for the SD) of H and λE. This supports the use of a local roughness length during stable conditions.

Comparison results for transition hours clearly show the improved skill concerning λE_{est} and especially H_{est} using the new scheme instead of UH85, as the SD and bias in the estimates of H are reduced from 16.4 and 9.8 to 10.3 and 3.1 W m^{-2}, respectively (profile method observations). The SD and bias in λE_{est} are improved from 18.1 and −8.6 to 15.0 and −1.1 W m^{-2}, respectively (balance method observations). In view of the

TABLE 4. Site-specific surface parameters. Between parentheses are the selections for short grass in the present and previous schemes.

New scheme	UH85 scheme
Albedo, r [Eq. (11)]	Albedo, r (0.23)
Emissivity, ε_s (0.94)	Emissivity, ε_s (1.0)
Roughness length for heat z_{0H} (0.001 m)	Empirical heating coefficient, C_H
Roughness length for momentum, z_{0M} [local (0.01 m) and effective]	Roughness length for momentum, z_{0M}
Soil heat transfer coefficient, A_G (5.0)	Soil heat transfer coefficient, A_G (5.0)
Surface resistance r_s with simplifications	Empirical coefficients, α (1.0) and β (0.033u_*)

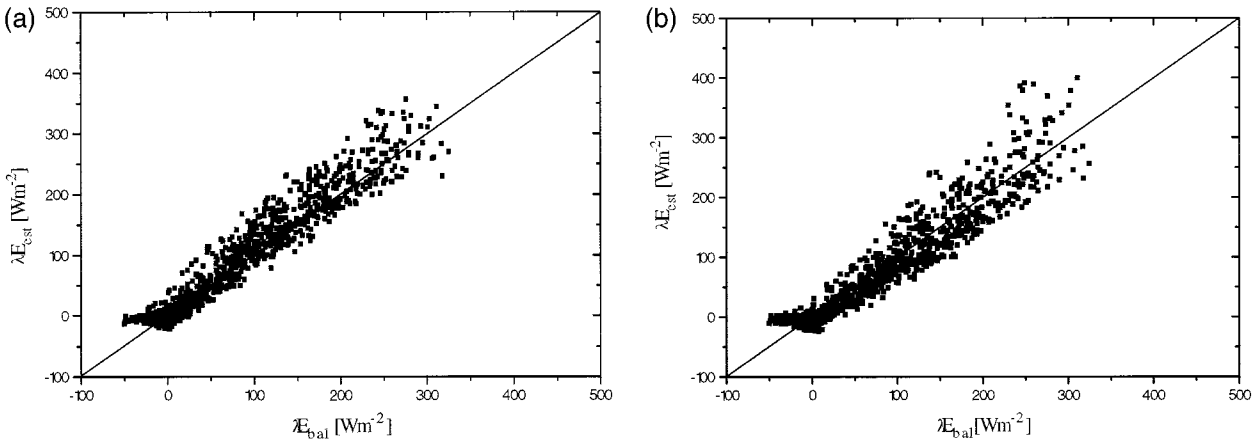

FIG. 9. (a) Comparison of the observed latent heat flux using the balance method (λE_{bal}) with estimates (λE_{est}) using the new scheme. The SD = 21.8 W m^{-2} (17.6 vs λE_{Bow}) and the bias = +6.3 W m^{-2} (+4.6 vs λE_{Bow}). (b) Comparison of the observed latent heat flux using the balance method (λE_{bal}) with estimates (λE_{est}) using the UH85 scheme. The SD = 24.5 W m^{-2} (19.6 vs λE_{Bow}) and the bias = −1.9 W m^{-2} (−3.7 vs λE_{Bow}).

average H_{prof} observed during transition hours (namely, −11.7 W m^{-2}; minimum value −68 and maximum value 0 W m^{-2}), the errors for H_{est} with the UH85 scheme are relatively large.

During daytime, unstable hours, the new scheme achieves better estimates for H (SD = 15.5 W m^{-2}) than the UH85 scheme (SD = 20.0 W m^{-2}). Moreover Fig. 8b illustrates the underestimation by the MPT approach at the upper range of the sensible heat flux (as already noticed in section 7). On the other hand, the results of both schemes for the latent heat flux are comparable. The new scheme produces a smaller SD (28.9 instead of 33.5 W m^{-2}), whereas the UH85 scheme provides a smaller bias in the estimated λE (−1.9 instead of +14.2 W m^{-2}). Part of the bias in the estimated latent heat fluxes with the new scheme may be due to errors in the observed G. As mentioned in section 6, high values of the observed G are probably overestimated, leading to an underestimation of $Q^* - G$. Because the observed $Q^* - G$ is used in the Bowen method as well as the balance method (section 3), the latent heat fluxes obtained with latter methods will also be underestimated. While in the Bowen method the bias in $Q^* - G$ is spread over H_{Bow} and λE_{Bow}, the complete underestimation in $Q^* - G$ is passed on to λE_{bal} in the balance method. Consistent with the hypothesis mentioned above, the average $\lambda E_{bal} < \lambda E_{Bow} < \lambda E_{prof}$. This is important for the evaluation of the surface fluxes in this section.

Besides the negative bias in G, an overestimation in $Q^* - G$ by the new scheme is caused by the positive bias in Q^*. During daytime unstable hours, about 4 of the 7 W m^{-2} offset in Q^* can be attributed to the use of the albedo formulation [(11), (12), (13)]. Apparently the albedo is too small during these hours. The rest of the bias in Q^* is associated with an overestimation of $L^{\downarrow}$ during daytime unstable hours. In the UH85 scheme, the large overestimation of Q^* during daytime with $r = 0.23$ is compensated by the bias in the estimated L_{net}. The use of an albedo formulation dependent on solar elevation (11) seems to be justified by the results, as the bias in Q^* increases from +6.99 to +12.30 W m^{-2} if a constant albedo is applied. Nevertheless, even if we apply a constant albedo, estimates of H and λE remain better with the new scheme (SD = 15.6 and 29.4 W m^{-2}, respectively).

The use of the fraction of middle and low cloud as an additional input variable in the new scheme results in better estimates of the surface fluxes, but without this extra variable the advantages with the new scheme remain present. For all hours (1453 cases during day and night), the bias against H_{prof} and λE_{bal} increases from +1.6 and 6.3 to 4.0 and 10.5 W m^{-2}, respectively (when we leave out N_h). However, the SD versus H_{prof} and λE_{bal} stays practically the same, as they increase from 11.8 and 21.8 to 12.0 and 22.0, respectively. For comparison, the SD for all hours with UH85 against H_{prof} and λE_{bal} is 15.6 and 24.5 W m^{-2}, respectively. It also appears that the surface flux estimates slightly improve when direct observations of $L^{\downarrow}$ are used (in addition to observations of $K^{\downarrow}$). For example, for all cases the SD for λE decreases to 19.4 W m^{-2}.

In summary, it can be stated that the surface fluxes (especially H) are improved with the new scheme. For the latent heat flux this improvement is most evident in the SD. The new scheme provides a smaller SD in the estimated ($Q^* - G$), whereas the bias is larger. The greater part of this bias in the new scheme might be explained by erroneous measurements of the soil heat flux (section 6).

9. Discussion and conclusions

In this paper we present an updated scheme that relates the surface fluxes of momentum and sensible and latent heat to weather variables, either measured routinely or predicted by forecast models. The scheme is

composed of parameterizations concerning the radiative components and the surface energy fluxes. The number of input variables and parameters to be specified are kept as small as possible. Together with alternatives, the parameterizations are evaluated, under many sorts of weather conditions, using 1 yr of observations above a grass-covered surface in Cabauw (BB97). This dataset is used both for comparison and parameterization purposes. Evaluation with an independent dataset would be desirable.

Emphasis is put on the problem of how to determine the surface temperature because of its crucial role in most parameterizations of the surface radiation and energy budget (section 4). Distinction is made between stable conditions, under which measurements at synoptic height appear to be in equilibrium with the local surface, and unstable conditions when measurements seem to be influenced by deviating upstream surface conditions.

Special attention is also paid to the parameterization of the latent heat flux. We basically examine two approaches (but with several alternatives) for the estimation of λE, namely, the PM and the MPT formulations. The MPT concept shows erroneous behavior at the upper and lower limit of the sensible heat flux. The lower limit is caused by the constant aerodynamic evaporation in the MPT concept, while the upper limit can be attributed to the temperature dependence of the term $[1 - s/(s + \gamma)]$. When using the PM concept for λE, the aerodynamic (r_a) and the surface resistance (r_s) need to be specified. The formulation of r_a is determined using the results of the surface temperature experiments in combination with Monin–Obukhov similarity theory. A combination of this r_a with an empirical formulation of the surface resistance (namely, $r_s = 10\Delta q_{2\mathrm{m}}$) achieves surprisingly good estimations of H and λE for the current 1-yr dataset. Examination of this very simple surface resistance formula for other datasets is strongly recommended.

The outputs of the proposed new scheme are compared with outputs of a previous approach (Holtslag and van Ulden 1983; van Ulden and Holtslag 1985). The main difference between both schemes concerns the parameterization of the latent heat flux and the treatment of the surface temperature. The new scheme applies a PM formulation, whereas the UH85 scheme uses the MPT concept. It appears that in particular the sensible heat flux H is improved with the new scheme.

Finally, one may ask: How general are the current findings and which parameters need adjustment for other sites? In Table 4 the site-specific surface parameters are recited. All the parameters in the new scheme are commonly applied and described in the literature for different surface covers and soil types. Therefore, we think it should be relatively easy to adjust the scheme for use above other surfaces. However, it is not clear at this stage that our simplification for r_s is generally applicable. Regarding the longwave downward radiation $L^{\downarrow}$, we think that a correction for high clouds and an emissivity including a vapor pressure dependence are preferable if no direct observations or more detailed estimates of $L^{\downarrow}$ are available. Similarly, we prefer the incoming solar radiation as measured or from the outputs of more detailed radiation calculations.

In view of the performance and the limited input variables, we conclude that the new scheme may be useful for many applications in boundary layer meteorology.

Acknowledgments. We are grateful to Anton Beljaars, Fred Bosveld, and Bart van den Hurk for many helpful discussions and suggestions. Comments on a draft of this paper by Bart van den Hurk, Jeanette Onvlee, Peter Duynkerke, and the three anonymous reviewers are gratefully acknowledged. Finally, we are indebted to Birgit van Diemen for the production of Fig. 1.

APPENDIX

The Algorithm of the New Scheme

The results of sections 4, 5, 6, and 7 are combined in a new scheme that provides the fluxes of sensible heat, latent heat, and momentum. The new scheme uses the following input:

- q_a (g kg^{-1}) at z_{q_a},
- T_a (°C) at z_{T_a},
- 24-h mean 2-m temperature (°C),
- u_a (m s^{-1}) at z_{u_a},
- $K^{\downarrow}$ (W m^{-2}), and
- $L^{\downarrow}$ (W m^{-2}) or N and N_h (fraction, 0–1).

The first step in the procedure is to make a first guess of friction velocity and aerodynamic resistance, assuming neutral conditions. As such

$$u_{*_{\mathrm{meso}}} = \frac{ku_a}{\ln(z_{u_a}/z_{0M\mathrm{eff}})} \tag{A1}$$

and

$$r_a = \frac{1}{u_{*_{\mathrm{meso}}}k}\ln\left(\frac{z_{T_a}}{z_{0H}}\right). \tag{A2}$$

Subsequently, a first guess of the sensible heat flux H can be made with

$$H = \frac{AD + B}{C + AE}, \tag{A3}$$

where $A = (s + \gamma^*)R - s(s + \gamma^*)$, $B = -(s + \gamma^*)$, $C = (s + \gamma^*)R$, $D = K^* + L^{\downarrow} + 3\varepsilon\sigma T_a^4 + A_G\overline{T}_{24\mathrm{h}} - (4\varepsilon\sigma T_a^3 + A_G)(T_a + \Gamma_d z_{T_a})$, and $E = (4\varepsilon\sigma T_a^3 + A_G)(r_a/\rho c_p)$, with $R \equiv [s + \gamma^*(1 + r_s/r_a)]$.

In the above, $s = (\partial e_s/\partial T_a)$, where e_s is the saturated vapor pressure (mb); $\gamma^* \equiv c_p(\lambda 0.622)^{-1}$ (mb °C^{-1}); $r_s = 10\Delta q_a$ (s m^{-1}) is the surface resistance; K^* is determined with (2), (11), (12), and (13); $L^{\downarrow}$ is either directly input or calculated according to section 5a, specifying

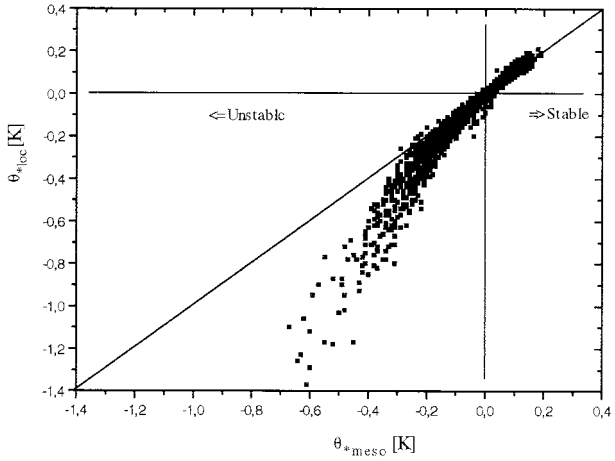

FIG. A1. Comparison of $\theta_{*\mathrm{loc}}$ (determined with Monin–Obukhov theory and observations of temperature and humidity at 2 and 0.6 m, wind speed at 10 m, and a local roughness length for momentum) with $\theta_{*\mathrm{meso}}$ (determined with Monin–Obukhov theory and observations of temperature and humidity at 10 and 0.6 m, wind speed at 10 m, and an effective roughness length for momentum) (6981 cases).

ε_s. Here $\overline{T_{24\mathrm{h}}}$ is the 24-h mean 2-m temperature (applied to the calculation of G, section 6), and $\Gamma_d = 0.01$ (K m^{-1}) is the adiabatic lapse rate.

The available energy can be written as

$$(Q^* - G) = D - EH. \tag{A4}$$

Now the potential temperature scale θ_* is determined with

$$\theta_{*_{\mathrm{meso}}} = \frac{-H}{\rho c_p u_{*_{\mathrm{meso}}}}. \tag{A5}$$

The temperature scale (A5) and the friction velocity (A1) are used to estimate the meso-Obukhov length:

$$L_{\mathrm{meso}} = \frac{u^2_{*_{\mathrm{meso}}} T_a}{kg\theta_{*_{\mathrm{meso}}}}. \tag{A6}$$

If $L_{\mathrm{meso}} > 0$, the above procedure is repeated with local parameters (i.e., $z_{0M\mathrm{loc}}$ instead of $z_{0M\mathrm{eff}}$) resulting in an estimate of L_{loc}. Note that a specific value of z_{0M} does not have impact on the sign of the stability. Now the main iteration loop starts and u_* and r_a and are estimated again, but this time including stability correction [(6), (7)]. It appears that usually only a few iterations are needed to achieve an accurate value of L. However, in very stable situations with low wind speed, the iteration fails. In that case L is fixed on $L = 2$ m. As a result, very small sensible and latent heat fluxes are produced (in agreement with observations). If $\lambda E < 0$ after the iteration, the iteration should be restarted with $r_s = 0$. However, by using $r_s = 10\Delta q_{2\mathrm{m}}$, the surface resistance is typically close to zero under conditions with $\lambda E < 0$.

In stable situations, the procedure mentioned above provides $u_{*_{\mathrm{loc}}}$. Yet, in order to transform wind from 10 m to higher altitudes, we rather need a mesoscale u_*. Hence an additional iteration is performed for stable situations only. First, $u_{*_{\mathrm{meso}}}$ is estimated with $z_{0M\mathrm{eff}}$ and L_{loc} resulting from the above iteration procedure using (6). Subsequently this $u_{*_{\mathrm{meso}}}$ is used, together with $\theta_{*_{\mathrm{loc}}}$, also from the previous iteration cycle, to estimate L_{meso} (A6). With the use of this L_{meso}, $u_{*_{\mathrm{meso}}}$ (6) is improved, and the procedure is repeated until L_{meso} obtains the required accuracy. Note that we use $\theta_{*_{\mathrm{loc}}}$ and not H_{est} for the determination of L_{meso}. According to Holtslag and De Bruin (1988), it is unlikely that H remains constant with height during nighttime, whereas the potential temperature scale is probably more invariant. This assumption is illustrated by Fig. A1, which reveals that $\theta_{*_{\mathrm{loc}}} \approx \theta_{*_{\mathrm{meso}}}$ during stable conditions. Note that $\theta_{*_{\mathrm{meso}}}$ is supposed to be valid at greater heights than $\theta_{*_{\mathrm{loc}}}$. In addition, we mention that a constant θ_* with height during stable conditions is consistent with the choice for a constant z_{0H} (sections 2 and 4).

REFERENCES

Baldocchi, D. B., R. J. Luxmoore, and J. L. Hatfield, 1991: Discerning the forest from the trees: An essay on scaling canopy stomatal conductance. *Agric. For. Meteor.,* **54,** 197–226.

Beljaars, A. C. M., 1987: The measurement of gustiness at routine wind stations—A review. WMO/IOM Rep. 31, Geneva, Switzerland, 50 pp.

——, and A. A. M. Holtslag, 1990: A software library for the calculation of surface fluxes over land and sea. *Environ. Software,* **5,** 60–68.

——, and ——, 1991: Flux parameterization over land surfaces for atmospheric models. *J. Appl. Meteor.,* **30,** 327–341.

——, and P. Viterbo, 1994: The sensitivity of winter evaporation to the formulation of aerodynamic resistance in the ECMWF model. *Bound.-Layer Meteor.,* **71,** 135–149.

——, and F. C. Bosveld, 1997: Cabauw data for the validation of land surface parametrization schemes. *J. Climate,* **10,** 1172–1193.

——, P. Schotanus, and F. T. M. Nieuwstadt, 1983: Surface layer similarity under non-uniform fetch conditions. *J. Climate Appl. Meteor.,* **22,** 1800–1810.

——, A. A. M. Holtslag, and R. M. van Westrhenen, 1989: Description of a software library for the calculation of surface fluxes. Tech. Rep. TR-112, KNMI, De Bilt, the Netherlands, 32 pp. [Available from Royal Netherlands Meteorological Institute, P. O. Box 201, 3730 AE, De Bilt, the Netherlands.]

Brutsaert, W. H., 1982: *Evaporation in the Atmosphere*. Reidel, 299 pp.

Chen, T. H., and Coauthors, 1997: Cabauw experimental results from the Project for Intercomparison of Land-surface Parameterization Schemes (PILPS). *J. Climate,* **10,** 1194–1215.

De Bruin, H. A. R., and A. A. M. Holtslag, 1982: A simple parameterization of the surface fluxes of sensible and latent heat during daytime compared with the Penman–Monteith concept. *J. Appl. Meteor.,* **21,** 1610–1621.

Duynkerke, P. G., 1992: The roughness length for heat and other vegetation parameters for a surface of short grass. *J. Appl. Meteor.,* **31,** 579–586.

Garratt, J. R., and B. B. Hicks, 1973: Momentum, heat and water vapor transfer to and from natural and artificial surfaces. *Quart. J. Roy. Meteor. Soc.,* **99,** 680–687.

——, and R. J. Francey, 1978: Bulk characteristics of heat transfer in the unstable, baroclinic atmospheric boundary layer. *Bound.-Layer Meteor.,* **15,** 399–421.

Goudriaan, J., and H. H. van Laar, 1994: *Modeling Potential Crop Growth Processes.* Kluwer Academic Publishers, 256 pp.

Holtslag, A. A. M, and A. P. van Ulden, 1983: A simple scheme for daytime estimates of the surface fluxes from routine weather data. *J. Climate Appl. Meteor.,* **22,** 517–529.

——, and F. T. M. Nieuwstadt, 1986: Scaling the atmosperic boundary layer. *Bound.-Layer Meteor.,* **36,** 201–209.

——, and H. A. R. De Bruin, 1988: Applied modeling of the nighttime surface energy balance over land. *J. Appl. Meteor.,* **27,** 689–704.

Jarvis, P. G., 1976: The interpretation of the variations in leaf water potential and stomatal conductance found in canopies in the field. *Philos. Trans. Roy. Soc. London,* **B273,** 593–610.

Monteith, J. L., 1981: Evaporation and surface temperature. *Quart. J. Roy. Meteor. Soc.,* **107,** 1–27.

——, 1995: Accomodation between transpiring vegetation and the convective boundary layer. *J. Hydrol.,* **166,** 251–263.

Nieuwstadt, F., 1978: The computation of the friction velocity u_* and the temperature scale T_* from temperature and wind velocity profiles by least squares methods. *Bound.-Layer Meteor.,* **14,** 235–246.

Oke, T. R., 1978: *Boundary Layer Climates.* Methuen, 372 pp.

Paltridge, G. W., and C. M. R. Platt, 1976: *Radiative Processes in Meteorology and Climatology.* Elsevier, 318 pp.

Priestley, C. H. B., and R. J. Taylor, 1972: On the assessment of surface heat flux and evaporation using large-scale parameters. *Mon. Wea. Rev.,* **100,** 81–92.

Slatyer, R. O., and I. C. McIlroy, 1961: *Practical Micrometeorology.* CSIRO, 310 pp.

van Ulden, A. P., and A. A. M Holtslag, 1985: Estimation of atmospheric boundary layer parameters for diffusion applications. *J. Climate Appl. Meteor.,* **24,** 1196–1207.

——, and J. Wieringa, 1996: Atmospheric boundary layer research at Cabauw. *Bound.-Layer Meteor.,* **78,** 39–69.

Wieringa, J., 1986: Roughness-dependent geographical interpolation of surface wind speed averages. *Quart. J. Roy. Meteor. Soc.,* **112,** 867–889.